Biomass and Bioenergy 217 (2027) 110093

Contents lists available at ScienceDirect

Biomass and Bioenergy

journal homepage: www.elsevier.com/locate/biombioe

Production of jet fuel precursors from the aldol condensation of lignocellulosic furfural and levulinic acid over tailored Zr-Al-beta catalysts

Natalia Uricochea [a,b], Jennifer Cueto [c], María del Mar Alonso-Doncel [c], Gabriel Morales [a,b], Marta Paniagua [a,b], Juan A. Melero [a,b,*]

[a] Chemical and Environmental Engineering Group, Universidad Rey Juan Carlos, c/Tulipán s/n, Móstoles, 28933, Spain
[b] Instituto de Investigación de Tecnologías para la Sostenibilidad (ITPS), Universidad Rey Juan Carlos, c/Tulipán s/n, Móstoles, 28933, Spain
[c] Thermochemical Processes Unit, IMDEA Energy Institute, Avda. Ramón de la Sagra, 3, Móstoles, 28935, Spain

ARTICLE INFO

Keywords:
Furfural
Levulinic acid
Aldol condensation
SAF precursors
Zr-Al-Beta zeolite

ABSTRACT

Herein, the aldol condensation of furfural (FAL) and levulinic acid (LA) toward the selective formation of β- and δ-furfurylidene-levulinic acid (C_{10} adducts) is investigated over a series of Zr-modified Beta zeolites under solvent-free conditions. Preliminary studies reveal that the parent commercial H-Beta zeolite exhibits limited performance, reaching low yield to C_{10} products due to strong Brønsted acidity promoting secondary reactions such as FAL polymerization. Progressive dealumination and Zr incorporation led to a marked increase in FAL conversion and C_{10} yield. The Zr/Al molar ratio, which governs the balance between Brønsted and Lewis acid sites, influences the catalytic activity and selectivity. Fully dealuminated Zr-Beta-4 catalyst was identified as the best-performing material in terms of FAL conversion, carbon balance, and yield/selectivity toward C_{10} adducts. Reaction time and temperature were simultaneously evaluated through a combined severity factor (CSF), achieving maximum selectivity and yield at intermediate CSF values (2.5 – 3). Subsequent optimization of reaction conditions, including LA/FAL molar ratio and FAL/catalyst mass ratio, demonstrated that operating at 120 °C provides the optimal compromise between activity and selectivity. Under optimized conditions (LA/FAL molar ratio = 6.8, FAL/Cat mass ratio = 2.5, 120 °C, 4 h), maximum response values of X_{FAL} = 75.2% and Y_{C10} = 48.8% were achieved. Catalyst reusability tests confirmed stable performance over three consecutive cycles without intermediate calcination, evidencing the robustness of Zr-Beta-4 catalyst. Overall, this study demonstrates that tuning zeolite acidity via controlled Al removal and Zr incorporation enables the efficient, stable, and solvent-free cross-aldol condensation of biomass-derived furfural and levulinic acid.

1. Introduction

Globally, air transport consumes approximately 3% of the world's fossil fuels and accounts for almost 14% of transport CO_2 emissions (approx. 3% of global GHG emissions) [1]. According to the European Environment Agency, this contribution is expected to increase 45% by 2035 if not corrective actions are taken [2]. European Union (EU) have established a wide variety of targets for the progressive decarbonization of the aviation sector with the purpose of achieving a global carbon neutrality by the second half of the 21st century [3]. In this context, the EU Refuel Aviation regulation (approved in 2023, October) obliges to gradually increase the blend of aviation sustainable fuel (SAFs) from 2% in 2025 up to 70% in 2050. SAFs include drop-in infrastructure-compatible aviation fuels that are either synthetic coming from captured CO_2 and renewable hydrogen (e-fuels) or advanced biofuels (bio-SAFs) produced from nonedible biogenic resources. These SAFs will play an important role in reaching the aviation industry's commitment of achieving net zero CO_2 emissions in 2050 [4].

Seven bio-SAFs production pathways are currently certified by ASTM for blending with conventional kerosene, up to a maximum limit of 50%. These approved technologies are Fischer-Tropsch synthetic paraffinic kerosene (FT-SPK); Fischer-Tropsch synthetic kerosene with aromatics (FT-SKA); direct sugar to hydrocarbon (DSHC) or synthesized iso-paraffins (SIP); hydrotreated esters and fatty acids (HEFA); alcohol to jet (ATJ); and catalytic hydro-thermolysis jet fuel (CHJ) [5–7].While the production of SAFs from lignocellulosic materials is still at the demonstration scale, triglyceride based HEFA jet fuel is currently commercialized. HEFA technologies require much lower capex than

* Corresponding author. Chemical and Environmental Engineering Group, Universidad Rey Juan Carlos, c/Tulipán s/n, Móstoles, 28933, Spain.
E-mail address: juan.melero@urjc.es (J.A. Melero).

https://doi.org/10.1016/j.biombioe.2026.110093
Received 15 June 2026; Received in revised form 9 September 2026; Accepted 10 September 2026
Available online 15 September 2026
0961-9534/© 2026 The Authors. Published by Elsevier Ltd. This is an open access article under the CC BY-NC license (http://creativecommons.org/licenses/by-nc/4.0/).

lignocellulose-based technologies, but its main shortcoming is the low availability of oleaginous feedstock to meet the growing SAFs demand. However, the number of studies on lignocellulose-based technologies is continuing to grow due to the larger availability of lignocellulosic wastes. Among these lignocellulose-based routes, the depolymerization of lignocellulose biomass into multifunctional platform chemicals is gaining a great interest in the literature [8]. Thus, furfural (FAL), levulinic acid (LA) and 5-hydroxymethyl furfural (5-HMF) are excellent candidates for obtaining long-chain aviation fuel precursors by means of C-C coupling reactions.

An important challenge is the design of heterogeneous catalysts to carry out these C-C coupling reactions with high selectivity and avoiding secondary reactions. In this study, the focus is on the aldol condensation of FAL and LA because both can be produced in a sustainable way from lignocellulosic wastes [9–11]. As shown in Scheme 1, two C_{10} isomeric condensation products, namely δ-furfurylidene-levulinic acid (δ-FDLA) and β-furfurylidene-levulinic acid (β-FDLA), are expected to be generated from the reaction of LA with FAL. For the production of jet-fuel range hydrocarbons, these adducts must be subsequently hydrodeoxygenated to remove oxygen and unsaturations.

Literature dealing with the FAL and LA condensation remains scarce. The first pioneering work was described in 2015 by Fan et al. using NaOH as catalyst [12,13], but suffering from the inherent drawbacks of the homogeneous catalysis. Afterwards, heterogeneous base and acid catalysts have been reported. A potassium-modified hierarchical MFI zeolite showed an outstanding activity and recyclability in the aldol condensation of LA with FAL in water, affording a complete FAL conversion and 70.6% yield of combined δ-FDLA and β-FDLA at 100 °C within 9 h [14]. Unlike base catalysts, acidic zeolites have also been exploited for converting LA with FAL into C_{10} products. Zhang et al. reported for the first time this reaction over acid zeolites but with FAL conversions below 40% and low selectivities, suggesting the uncontrolled presence of excessive undesired reactions [15]. Ordoñez et al. performed a deep study over zeolite catalysts, optimizing reaction conditions and showing that commercial ZSM-5 zeolite (Si/Al 23) can afford 50% yield (combined δ-FDLA and β-FDLA) at 150 °C in a highly selective manner [16]. More recently, the same group reported the use of aluminosilicate mesoporous materials containing weak acid sites. This catalytic system achieves yields around 50% with selectivities close to 100%, similar to the previously reported ZSM-5 material [17]. Noteworthy, to prevent side reactions such as cyclization the reported studies have been carried out in aqueous medium and using an inorganic salt (Na_2CO_3) to neutralize the carboxylic groups in LA. However, this implies the necessity of re-acidifying the resultant product, accompanied by the disposal of the corresponding salts, which introduces new potential environmental issues. On the other hand, the modulation of the acid sites strength has been identified as a key parameter to prevent side reactions and maximize selectivity to the target oxygenated adducts.

Herein, we report the aldol condensation of FAL with LA towards the selective formation of β- or δ-FDLA over tailored Zr-modified Beta catalysts in a solvent-free medium, avoiding the neutralization and reacidification steps necessary in aqueous systems. Furthermore, avoiding the use of solvents is very interesting not only the from the point of view of down-stream separation costs, but also from an environmental perspective. Special attention is given to the impact of the Zr/Al molar ratio of the different catalysts, which corresponds to different loadings of Brønsted and Lewis acid sites, on the selectivity. Additionally, reactions conditions are optimized for the best-performing catalyst, and its reusability is evaluated.

2. Experimental section

2.1. Materials

Levulinic acid (LA, 98%, Sigma-Aldrich) and furfural (FAL, 99%, Sigma-Aldrich) were used as reagents in the aldol condensation reaction. n-Decane (>99%, Thermo Scientific) was added as internal standard, and ethyl acetate (>99.5%, Sigma-Aldrich) was employed as the analytical solvent. The zeolite used as starting material was a commercial H-Beta zeolite (CP 814C, Zeolyst). Nitric acid (HNO_3, 65%, Sigma-Aldrich) was required to remove the aluminium content from the commercial catalyst, and zirconium (IV) nitrate ($Zr(NO_3)_4$, Chemicalpoint) was used as the precursor for the zirconium incorporation process. Monoclinic-phase zirconium(IV) oxide (ZrO_2, Sigma Aldrich) was used as a commercial reference catalyst.

2.2. Catalyst preparation

Several Zr-modified Beta materials were synthesized from a commercial H-Beta zeolite following a procedure previously reported in the literature [18]. The series includes materials with progressively increasing Zr/(Zr + Al) molar ratios, as well as a fully dealuminated sample in which the framework Al was completely replaced by Zr. Before modification, the commercial H-Beta zeolite was calcined at 550 °C for 6 h using a heating rate of 1.8 °C·min^{-1}. Controlled dealumination was then carried out using nitric acid solutions of different concentrations (0.3, 2, 5, and 10 M) selected according to the desired degree of Al removal. For each synthesis, 20 ml of the corresponding acid solution per gram of zeolite were added, and the suspension was stirred at RT for 1 h to achieve partial dealumination. Complete Al removal was achieved by treating the parent H-Beta zeolite with a 10 M nitric acid solution under reflux at 100 °C for 20 h. After the acid treatment, all samples were recovered by centrifugation and washed with deionized water until a neutral pH was reached. The resulting solids were then dried overnight at 100 °C. Subsequently, Zr was introduced by wet impregnation using an aqueous solution of $Zr(NO_3)_4$. The amount of Zr precursor added to each material was calculated based on the equivalent molar amount of Al removed during the dealumination step (checked by ICP-OES). After impregnation, the water was evaporated, and the solids were dried overnight and calcined in air following a two-steps procedure: 200 °C for 6 h, and 550 °C for an additional 6 h period, using a heating rate of 3 °C·min^{-1} for both steps. The resulting Zr-modified Beta catalysts were denoted as Zr-Beta-*n*., where *n* stands for a consecutive integer (see Table 1).

2.3. Catalyst characterization

Inductively Coupled Plasma-Optical Emission Spectroscopy (ICP-OES) using a Varian Vista AX apparatus was performed to determine the Al and Zr contents of the synthesized Zr-materials. The speciation of Al was analysed by solid-state ^{27}Al MAS NMR on a Bruker Advance III/HD 400 spectrometer equipped with a 4 mm MAS probe operating at

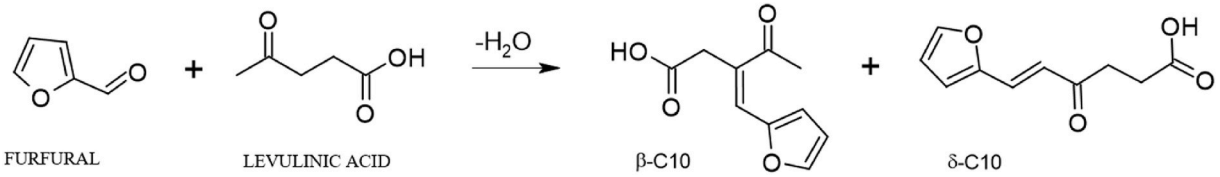

Scheme 1. Simplified scheme of the conversion of LA with FAL into bio-jet fuel precursors via aldol condensation.

Table 1
Composition, textural properties and acidity of parent H-Beta and Zr-modified Beta zeolites.

Catalysts[a]	Composition[b]				Textural properties			Acidic properties		
	Al (wt%)	Zr (wt%)	Si/Al	Zr/(Zr + Al)	S_{BET}[c] ($m^2 \cdot g^{-1}$)		V_p[d] ($cm^3 \cdot g^{-1}$)	Capacity[e] (mmol $H^+ \cdot g^{-1}$)	T_{max}[f] (°C)	B/L ratio[g]
					S_{EXT}	$S_{\mu p}$				
H-Beta	1.49	0.00	29.3	0.00	139	576	0.37	0.49	313	1.55
Zr-Beta-1	0.88	1.72	48.9	0.37	125	386	0.30	0.47	311	-
Zr-Beta-2	0.58	2.64	74.5	0.58	129	344	0.28	0.44	302	0.63
Zr-Beta-3	0.46	3.35	93.2	0.69	105	267	0.22	0.37	294	-
Zr-Beta-4	0.06	4.00	696.7	0.95	107	289	0.25	0.13	254	0.10

[a] Dealumination conditions: 0.3, 2, and 5 M nitric acid, 1 h, RT for Zr-Beta-1, Zr-Beta-2, and Zr-Beta-3, respectively; 10 M nitric acid, 24 h, 100 °C for Zr-Beta-4.
[b] Al, Zr (wt%); Si/Al, Zr/(Zr + Al) (atomic ratio) determined by ICP-OES.
[c] External surface area and micropores area calculated with the t-Plot method.
[d] Total pore volume recorded at $P/P_0 = 0.975$.
[e] Total acid capacity determined using NH_3-TPD.
[f] Temperature of the maximum desorption of NH_3 analysed by NH_3-TPD.
[g] Brønsted/Lewis acid sites ratio evaluated by pyridine FTIR (meq/meq).

9.4 T. To determine the crystallinity of the samples powder X-ray diffraction (XRD) patterns were collected in a Philips Xpert diffractometer using the Cu Kα line in the 2θ angle range of 5 – 50° with a step size of 0.04°. Textural properties were calculated from nitrogen adsorption-desorption isotherms at 77 K utilizing a Micromeritics TriStar 3000 equipment. BJH model was used for the analysis of data and total pore volume was taken at $P/P_0 = 0.975$. External surface area and micropores area were calculated with the *t*-Plot method. The acidity of the catalysts was assessed through ammonia temperature-programmed desorption (NH_3-TPD), carried out on a Micromeritics AUTOCHEM 2910 equipped with a thermal conductivity detector (TCD). In a typical run, 0.1 g of sample was pretreated at 300 °C under a helium flow (50 ml min^{-1}) for 1 h to remove adsorbed species. The system was then cooled to 100 °C, after which a 10 vol% NH_3/He mixture was introduced for 30 min to allow adsorption. Excess physisorbed ammonia was purged with helium, and the desorption profile was subsequently recorded by heating the sample up to 650 °C under the same He flow. Total acidity was determined by quantifying the integrated area of each desorption profile and applying the NH_3 calibration. To differentiate between weak, medium, and strong acid sites, the overall desorption curve was deconvoluted into individual Gaussian components. The concentrations of Brønsted (BAS) and Lewis (LAS) acid sites were determined using pyridine as a probe molecule, monitored by FTIR in a custom-built setup. Self-supported wafers (17.5 ± 1.5 mg cm^{-2}) were prepared and activated under high vacuum ($<10^{-4}$ mbar) at 480 °C for 2 h prior to pyridine injection. Then, the adsorption of the probe molecule was carried out at 150 °C, with the system sealed for 30 min to ensure equilibrium. Thermal desorption was then performed under high vacuum at 150 °C for 30 min before spectral acquisition. Additional measurements were conducted at 250 °C, 350 °C, and 450 °C, applying the same equilibrium time before recording the spectra. Data was collected on a Jasco-4600 spectrometer equipped with a TGS detector, with a spectral resolution of 4 cm^{-1} and 128 scans. The integrated molar extinction coefficients reported by Zholobenko et al. for the Beta zeolite were applied to the corresponding band areas for quantification: $\xi_{BAS} = 1.12$ cm μmol^{-1} at 1545 cm^{-1} and $\xi_{LAS} = 1.71$ cm μmol^{-1} at 1455 cm^{-1} [19].

2.4. Reaction procedure

The aldol condensation of FAL and LA was carried out in glass reactors (20 mL) using a Radleys Carousel stirring hot plate, equipped with temperature control and constant magnetic agitation at 400 rpm. In a typical run, the catalyst was first introduced in the reactor, followed by the addition of LA and FAL under solvent-free conditions. The reactors were then sealed and placed in the carousel for a predetermined time at a desired temperature. After each reaction, n-decane (0.1 g) was added as an internal standard, and ethyl acetate (20 mL) was subsequently introduced to homogenize the reaction mixture and prepare the samples for gas chromatography analysis. Catalyst reusability was evaluated through consecutive experiments in which the spent catalyst was recovered by simple filtration, washed with acetone at RT to remove residual reaction media, and dried at 110 °C prior to being reused in subsequent reaction runs.

2.5. Catalytic performance evaluation

Products identification was performed by GC-MS using an Agilent 5977B GC/MSD system equipped with a 30 m HP-5MS UI capillary column, based on information reported in previous studies [17]. Quantitative analysis was carried out by GC using an Agilent Intuvo 9000 fitted with a 30 m Agilent DB-5 capillary column and a flame ionization detector (FID). FAL and LA were calibrated using n-decane as internal standard, while non-commercially available C_{10} condensation products were quantified using the Effective Carbon Number (ECN) concept [20]. Additional details regarding the calculation of the ECN, the corresponding correction coefficients, and the estimation of response factors for the C_{10} condensation products are provided in the Supplementary Information (Table S1).

The catalytic performance was evaluated in terms of FAL conversion (X_{FAL}), yield towards the desired C_{10} aldol condensation products (Y_{C10}), selectivity to C_{10} adducts (S_{C10}), turnover frequency (TOF), carbon balance (CB) and combined severity factor (CSF). These parameters were calculated according to the following expressions:

$$X_{FAL}(\%) = \frac{Reacted\ moles\ of\ FAL}{Initial\ moles\ of\ FAL} \cdot 100 \quad [1]$$

$$Y_{C10}(\%) = \frac{Moles\ of\ product\ C10}{Initial\ moles\ of\ FAL} \cdot 100 \quad [2]$$

$$S_{C10}(\%) = \frac{Y_{C10}}{X_{FAL}} \cdot 100 \quad [3]$$

$$TOF = \frac{Moles\ of\ product\ C10}{Moles\ of\ Al + Zr\ in\ catalyst} \quad [4]$$

$$CB\ (\%) = \frac{10 * (moles\ of\ product\ C10) + 5 * (moles\ FAL + moles\ LA)}{5 * (initial\ moles\ of\ FAL + initial\ moles\ of\ LA)} \cdot 100 \quad [5]$$

$$CSF\ (\%) = log\left(t \cdot exp^{\frac{T-T_0}{14.75}}\right) \quad [6]$$

where t is the reaction time (min), T is the temperature (°C), T_0 is the reference temperature (100 °C) [17].

Both β- and δ-furfurylidene levulinic acid (Scheme 1) are C10 oxygenated intermediates that would subsequently undergo hydrodeoxygenation to produce fuel-range hydrocarbons with similar carbon numbers and physicochemical characteristics. Therefore, from the perspective of sustainable aviation fuel production, the overall yield of C10 condensation products is considerably more relevant than the β/δ isomer ratio.

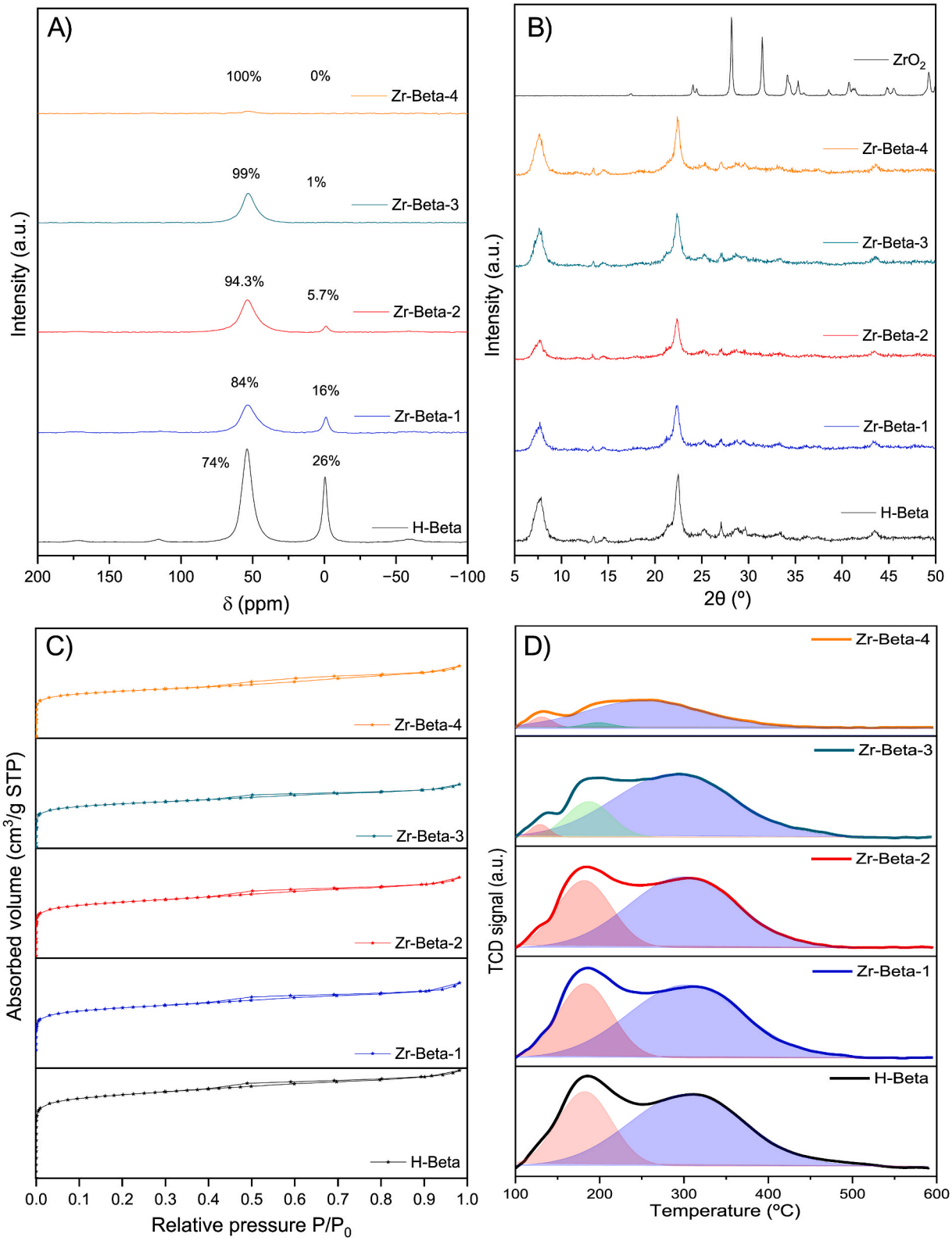

Fig. 1. Characterization of parent H-Beta and Zr-modified Beta zeolites: A) solid-state ^{27}Al NMR spectra; B) wide-angle XRD patterns; C) nitrogen (−196.15 °C) adsorption-desorption isotherms; D) NH_3-TPD analysis.

3. Results and discussion

3.1. Catalysts characterization

Starting from a commercial Beta zeolite, four Zr-modified Beta catalysts with different Zr/(Zr + Al) ratios were synthesized. Table 1 summarizes the most relevant physicochemical properties, including their composition, textural parameters, and acidic properties, for the series of Zr-modified Beta zeolites together with the parent commercial H-Beta zeolite used as reference. As can be observed, progressive dealumination was achieved across the series, with the Al content decreasing from 1.49 wt% in the parent H-Beta zeolite to 0.06 wt% in the fully dealuminated material. In turn, Zr was incorporated in the range of 1.72 – 4.00 wt%. The material synthesized under the most aggressive conditions (Zr-Beta-4) exhibits a dealumination degree over 95%, leading to a very high Si/Al ratio. These results confirm that a range of Zr-modified Beta zeolites, with Zr/(Zr + Al) ratios from 0 to 1, was successfully obtained.

To evaluate the coordination environment of the Al species removed during the synthesis, solid state ^{27}Al NMR spectroscopy was performed. Upon dealumination, extra-framework Al species with octahedral coordination (≈0 ppm) are preferentially removed compared to framework tetrahedrally coordinated Al species (≈55 ppm) (Fig. 1A). As a result, at high degrees of dealumination, the remaining Al is predominantly tetrahedrally coordinated. Furthermore, the almost complete removal of Al in the Zr-Beta-4 material is confirmed in the NMR spectra, in agreement with the ICP-OES compositional analysis.

To assess the crystallinity, X-ray diffraction (XRD) analyses were performed on the synthesized materials, the parent H-Beta zeolite, and crystalline ZrO_2 as a reference. The diffraction patterns confirm that the crystalline structure is preserved after dealumination and Zr incorporation for all the prepared materials (Fig. 1B). Nevertheless, the Zr-Beta samples exhibit a slight decrease in diffraction peak intensity together with peak broadening, which may arise from lattice distortions caused by both the dealumination process and the incorporation of Zr species into the zeolite framework. Importantly, no diffraction peaks attributable to ZrO_2 are detected, indicating effective dispersion of Zr species within the zeolite framework.

To gain further insight into the nature of the zirconium species, XPS analysis was performed on the Zr-Beta-4 sample, which exhibits the highest zirconium loading. As shown in Fig. S1, the Zr 3d binding energies are shifted towards higher values compared with bulk ZrO_2. This positive shift indicates that zirconium is located in a chemical environment different from that of crystalline zirconia and is strongly influenced by its interaction with the zeolitic matrix. These results support the presence of highly dispersed zirconium species strongly associated with the zeolite structure rather than segregated bulk zirconia domains. Although the available characterization does not allow an unequivocal distinction between framework and all possible extra-framework zirconium species, it clearly indicates that zirconium is present in a coordination environment different from that of bulk ZrO_2.

The textural properties of the materials were evaluated by nitrogen (−196.15 °C) adsorption-desorption measurements, which exhibit typical Type-1 isotherms characteristic of microporous materials (Fig. 1C). The slight slope of the isotherm in the relative pressure range of approximately 0.2 - 0.85 suggests only a minor contribution of mesoporosity, indicating that the dealumination treatment has a limited impact on mesopore formation. Consistently, no well-defined hysteresis loop is observed, further supporting the absence of significant mesoporosity. As shown in Table 1, the parent H-Beta zeolite displays a notably high total BET surface area, mainly associated with a large micropore surface area, while only a smaller contribution arises from the external surface area. As the Zr content in the materials increases, a progressive decrease in the BET surface area is observed, affecting predominantly the micropore surface area rather than the external surface area. Nevertheless, the $S_{\mu p}/S_{BET}$ ratio remains within a narrow range (0.80 - 0.73), indicating again that mesoporosity generation through dealumination is only marginally present. At the same time, a slight decrease in pore volume is detected, which may be attributed to partial pore blockage and/or surface coverage effects caused by the incorporation of Zr species within the zeolite channels.

To complete the characterization of the materials, evaluation of their acidic properties is essential, as acidity provides the functional features of the catalysts and plays a key role in governing their catalytic activity. As previously observed during the synthesis process, most of the catalysts retain a certain amount of Al while Zr is incorporated into the zeolite structure. The NH_3-TPD technique allows simultaneous assessment of both the concentration and the strength of the acid sites. Although zirconium incorporation introduces new Lewis acid sites, these sites interact differently with ammonia and generally exhibit weaker acidity than the original Al-related acid sites [21–23]. Fig. 1D displays the NH_3 desorption profiles of the commercial H-Beta zeolite and the Zr-modified Beta materials. As Al is progressively removed and Zr is incorporated, a decrease in the total number of acid sites is observed, as evidenced by the reduction in the area under the desorption curves (Table 1, Capacity). This decrease is particularly pronounced between the Zr-Beta-3 and Zr-Beta-4 materials, which is consistent with the larger reduction in Al content resulting from the more aggressive dealumination procedure applied to the latter. Additionally, three distinct desorption peaks are observed at approximately 130 °C, 180 °C, and 300 °C, corresponding to weak, medium, and strong acid sites, respectively, with higher desorption temperatures indicating stronger acid strength. After deconvolution of the profiles, the acid capacity associated with strong acid sites (300 °C) decreases from 0.32 to 0.12 mmol $H^+ \cdot g^{-1}$, while that of the medium-strength sites (180 °C) decreases from 0.15 to 0.01 mmol $NH_3 \cdot g^{-1}$. In addition, as shown in Fig. 1D and Table 1, an increase in the Zr/(Zr + Al) ratio leads to a shift of the maximum desorption temperature toward lower values, indicating a progressive decrease in the acid strength of the materials. As observed for the total number of acid sites, a clear shift of the desorption peaks toward lower temperatures is also evident between the Zr-Beta-3 and Zr-Beta-4 samples (Table 1). Thus, based on the NH_3-TPD results, it can be concluded that Al removal combined with Zr incorporation into the zeolite framework not only reduces the total acid capacity but also weakens the strength of the remaining acid sites.

3.2. Preliminary tests

Previous studies have demonstrated the potential of the BEA zeolite framework in the transformation of biomass into various high value-added products [24–27]. In the present work, its catalytic activity in the aldol condensation between FAL and LA is investigated. To evaluate the effect of different reaction parameters, including LA/FAL molar ratio, FAL/CAT mass ratio, and temperature, a series of exploratory reactions were carried out using the commercial H-Beta zeolite as reference catalyst at a fixed reaction time of 4 h (Fig. 2).

First, the LA/FAL molar ratio was varied in the range of 1-10 while keeping constant the temperature (120 °C) and the catalyst loading (FAL/CAT = 5). As shown in Fig. 2A, increasing the LA/FAL ratio leads to higher FAL conversion ($X_{FAL} = 37\%$), and higher yields ($Y_{C10} = 14\%$) to the desired aldol condensation products, with the yield stabilizing at LA/FAL ratios above 5. Therefore, a more diluted reaction medium favours improved conversion and products yield, likely due to the minimization of side reactions originating from FAL, such as FAL polymerization reactions, or from non-reversible adsorption on the catalyst surface. Next, the effect of catalyst loading was investigated by varying the FAL/CAT mass ratio between 1 and 5, while keeping constant the reactants ratio (LA/FAL = 1) and the temperature (120 °C) (Fig. 2B). In this case, as expected, a decrease in the amount of catalyst used leads to a reduction in both FAL conversion and yield toward the C_{10} condensation products. Therefore, the highest conversions ($X_{FAL} = 42\%$), and yields ($Y_{C10} = 15\%$) are obtained at the lowest FAL/

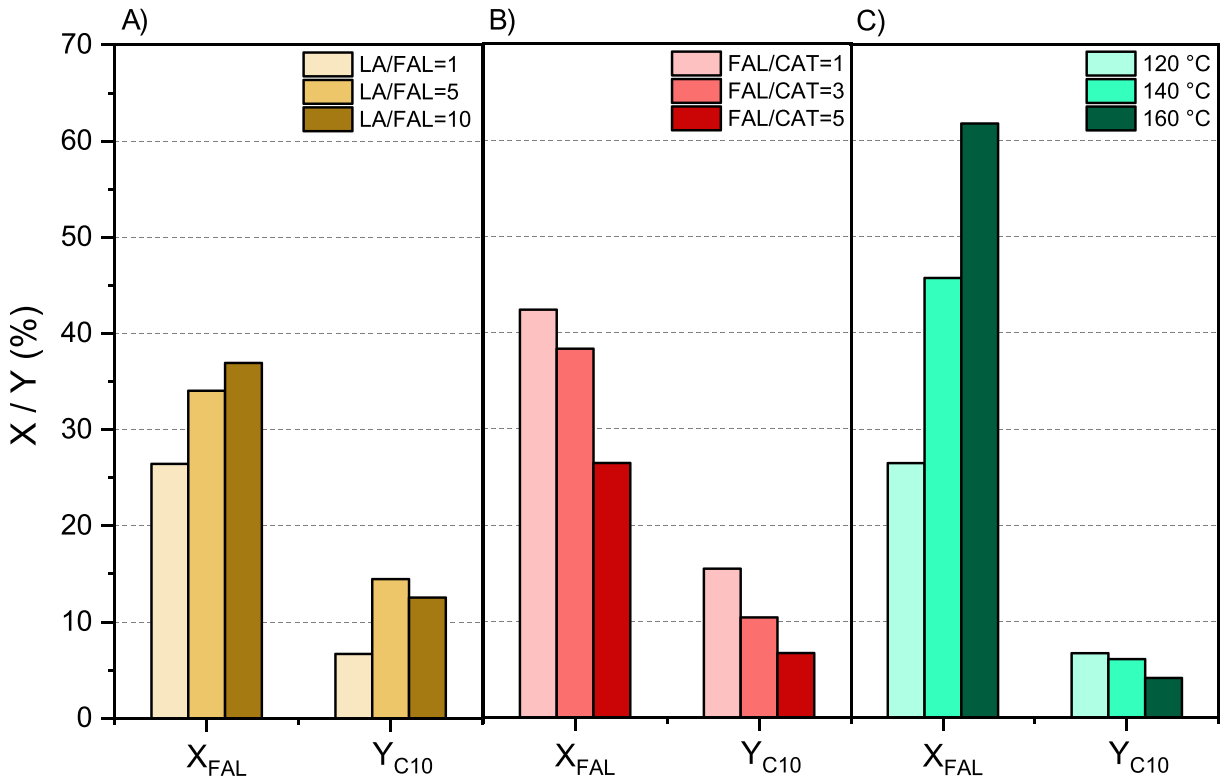

Fig. 2. Catalytic performance of commercial H-Beta zeolite on the catalytic aldol condensation of FAL and LA after 4 h of reaction. A) Effect of LA/FAL molar ratio (FAL/CAT mass ratio = 5; T = 120 °C); B) Effect of FAL/CAT mass ratio (LA/FAL molar ratio = 1; T = 120 °C); C) Effect of temperature (LA/FAL molar ratio = 1; FAL/CAT mass ratio = 5).

CAT mass ratio (FAL/CAT = 1). Lower FAL/CAT ratios were not explored, as this would require excessively high catalyst loadings, which could negatively affect stirring efficiency and mass transfer due to the high solid content of the reaction mixture. Finally, the effect of reaction temperature was examined by increasing it up to 160 °C, while keeping constant the reactants ratio (LA/FAL = 1) and the catalyst loading (FAL/CAT = 5) (Fig. 2C). The results show that higher temperatures enhance the catalytic activity, leading to increased FAL conversion (X_{FAL} = 62%).

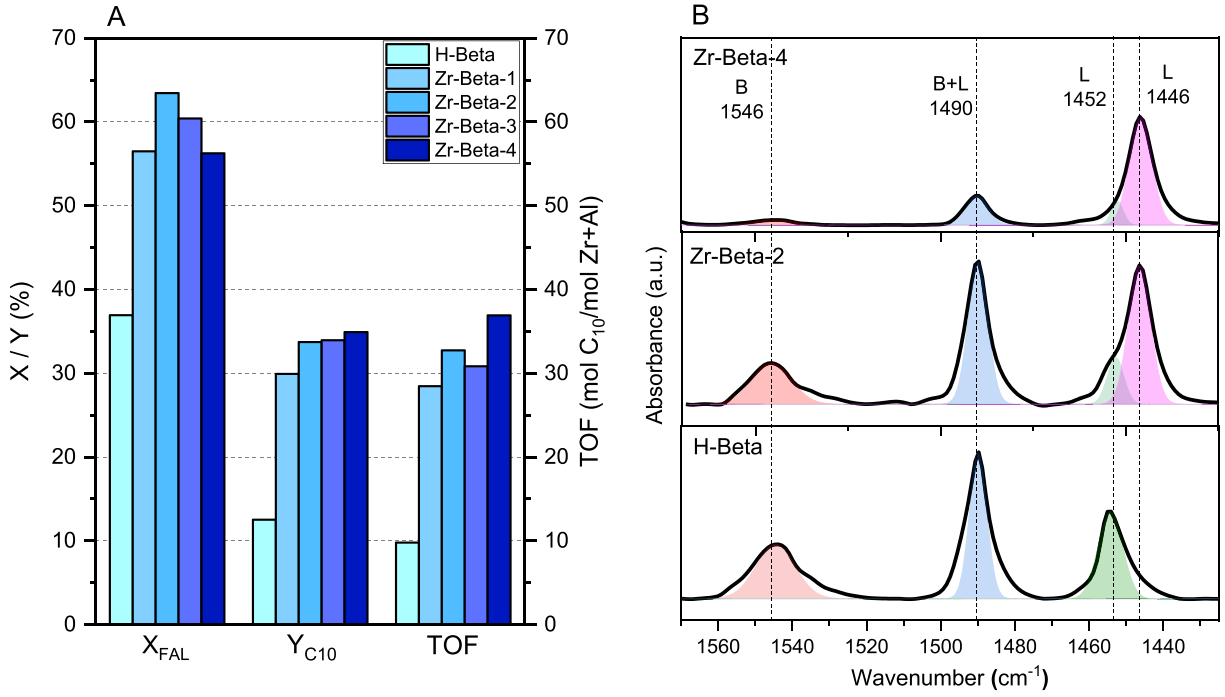

Fig. 3. A) Aldol condensation of FAL and LA over parent H-Beta zeolite and Zr-modified Beta zeolites in terms of FAL conversion (X_{FAL}), yield to desired condensation products (Y_{C10}), and TOF values. Reaction conditions: LA/FAL (mol/mol) = 10, FAL/CAT (wt/wt) = 5, T = 120 °C, t = 4 h. B) FTIR spectra obtained after pyridine desorption at 150 °C on H-Beta, Zr-Beta-2 and Zr-Beta-4.

However, high yields toward the desired aldol condensation products are not achieved under these conditions ($Y_{C10} < 7\%$), indicating that raised temperatures promote competing side reactions, such as FAL polymerization, rather than the aldol condensation of FAL and LA.

Based on these preliminary studies, it can be concluded that the catalytic activity of the commercial H-Beta zeolite in the aldol condensation of FAL and LA is rather limited, yielding only moderate amounts of the desired C_{10} condensation products under the operating conditions investigated. The strong Brønsted acidity associated with this commercial zeolite promotes competing FAL secondary reactions, as previously reported in the literature [28–30]. Therefore, in the following section, the aim is to improve the catalytic performance of this material by removing Al and incorporating Zr, which allows tuning the acidic properties of the resulting catalysts.

3.3. Screening of Zr-modified beta zeolites

To evaluate the effect of the Zr/(Zr + Al) ratio in the catalytic behaviour, the series of Zr-modified Beta zeolites synthesized were tested in the aldol condensation of FAL and LA (Fig. 3A). Considering the results over H-Beta zeolite (Fig. 2), reaction conditions were selected with the aim of minimizing undesired secondary reactions. Accordingly, the reaction was carried out under FAL diluted conditions (LA/FAL = 10) and at a relatively low reaction temperature (120 °C). In addition, in order to enable a more reliable comparison among the different catalysts, a low catalyst loading was employed (FAL/CAT = 5).

Data shown in Fig. 3A indicates that FAL conversion increases as the Al content decreases and the Zr content increases, until it reaches a plateau at values around 60%. Moreover, this increase in conversion is accompanied by a corresponding rise in yield toward the desired C_{10} products, reaching values above 30%. In order to compare the intrinsic catalytic activity of the different materials, the yield towards C_{10} products was normalized by the total amount of heteroatoms (Al + Zr) present in the catalyst, considering that both species may contribute to the generation of catalytically relevant acid sites. The resulting TOF values are included in Fig. 3A. The trend observed for these values is like that found for the C_{10} yield, confirming that the progressive substitution of Al by Zr enhances not only the overall catalytic performance but also the effectiveness of the catalytic centres.

This behaviour can be explained by the modification of the acidic properties of the material. As shown by the data reported in Table 1, increasing the Si/Al ratio leads to a decrease in the total number of acid sites, together with a reduction in acid strength, as determined by NH_3-TPD. In addition, the nature of the acid sites was evaluated by Fourier transform infrared spectroscopy (FTIR) using pyridine as a probe molecule (Fig. 3B). Owing to its basic character, pyridine allows discrimination between Brønsted and Lewis acid sites based on its specific interactions with each type of acid site. Three characteristic absorption bands were identified: pyridinium ion (PyH^+) interacting with Brønsted acid sites at 1546 cm^{-1}, a band at 1490 cm^{-1}, attributed to the simultaneous interaction of pyridine with both Brønsted and Lewis acid sites, and the interaction of pyridine with Lewis acid sites at 1445 - 1455 cm^{-1}. For this analysis, catalysts representing the extremes of the series were selected, the commercial H-Beta zeolite and the fully dealuminated Zr-Beta-4 sample, together with an intermediate material, Zr-Beta-2, with a moderate Zr/(Zr + Al) ratio. The acidity characterization reveals the presence of Brønsted type acid sites associated with the charge deficit generated by framework Al, together with Lewis acid sites that may arise from Al species in distorted, extra-framework or framework-associated environments and, in the Zr-Beta samples, from incorporated Zr species. In the Zr-Beta samples, this Lewis acid region can be deconvoluted into two contributions, located at 1452 and 1446 cm^{-1}. The band at 1452 cm^{-1} is mainly ascribed to Al-derived Lewis acid sites, whereas the contribution at 1446 cm^{-1} appears only in the Zr-containing samples and is tentatively assigned to Lewis acid sites associated with incorporated Zr species. Notably, the intensity of the 1446 cm^{-1} contribution increases with Zr loading, while that of the 1452 cm^{-1} band progressively decreases, in agreement with the removal of Al species upon dealumination. Nevertheless, some overlap between Zr- and Al-related Lewis acid contributions cannot be ruled out, since dealumination and Zr incorporation may distort the local environment of residual Al species, and framework-associated Al species may also contribute to weak Lewis acidity. The Brønsted to Lewis (B/L) acid site ratio was calculated, showing a marked decrease from 1.55 for H-Beta to 0.10 for Zr-Beta-4 (Table 1).

By correlating the catalytic performance with the acidic properties of the catalysts, an enhanced formation of the desired C_{10} aldol condensation products is observed as the Brønsted to Lewis (B/L) acid site ratio decreases. Lewis acid sites generated in Zr-containing Beta zeolites promote the activation of carbonyl compounds and facilitate the formation of the reaction intermediates involved in the aldol condensation pathway [31,32]. At the same time, the lower Brønsted/Lewis acid site ratio minimizes furfural oligomerisation and polymerization reactions, leading to higher selectivity towards the desired C10 condensation products.

On the other hand, the analysis of the textural properties of the modified materials (Table 1) shows that, although a progressive loss of microporous surface area and pore volume is observed as the Zr/(Zr + Al) ratio increases, these changes do not negatively affect catalytic activity. This observation suggests that the reduction in microporosity does not constitute a limiting factor for the aldol condensation reaction under the conditions investigated.

3.4. Optimization of the reaction conditions

3.4.1. Effect of the reaction time and the temperature

In order to study the effect of the reaction time and the temperature, a combined severity factor (CSF) previously employed in literature was used [17]. This factor allows to simultaneously analyse both variables, as they are closely interrelated with the severity of the reaction. With the aim of finding out the effect in the catalytic performance of this coefficient, several runs were made at different reaction times (in the range of 0.5 – 24 h) and temperatures (in the range of 100 – 140 °C). The CSF values resulting of the different combinations, calculated according to Eq. [6], are shown in Table S2. All reactions were carried out using a LA/FAL molar ratio of 1 to avoid the effect of reaction dilution, and a FAL/CAT mass ratio of 5 to allow for an adequate discrimination between the catalysts and also to minimize diffusional limitations within the reaction system. From the series of catalysts shown in Table 1, the extreme cases were selected: the Zr-free commercial H-Beta zeolite and the fully dealuminated H-Beta-4 zeolite, together with a catalyst exhibiting an intermediate Zr/(Zr + Al) ratio, H-Beta-2.

As shown in Fig. 4A, operating under more severe conditions leads to an increase in FAL conversion, as expected. Higher temperatures or longer reaction times promote the transformation of FAL into other compounds. The Zr-modified catalysts clearly exhibit higher FAL conversion values, with the fully dealuminated material showing the highest conversion across all CSF levels tested. However, a higher FAL conversion does not necessarily correlate with increased formation of the desired adducts. When focusing on the carbon balance (CB) values (Fig. 4B), it is observed that as the severity factor increases, CB becomes poorer, indicating the formation of a higher proportion of undesired by-products. The unidentified fraction is mainly attributed to furfural-derived oligomeric and polymeric species, as commonly reported in the literature for the aldol condensation of furfural and levulinic acid [33–36]. Their formation becomes increasingly important under severe reaction conditions, as evidenced by the progressive decrease in carbon balance. A particularly accelerated decrease in CB is observed for CSF values above 3 for all catalysts, with a more pronounced decline in the case of the H-Beta-4 catalyst. These results highlight two important aspects: i) the relevance of operating under mild conditions at the selected LA/FAL molar ratio and catalyst loading; ii) for Zr-Beta-4 (the catalyst

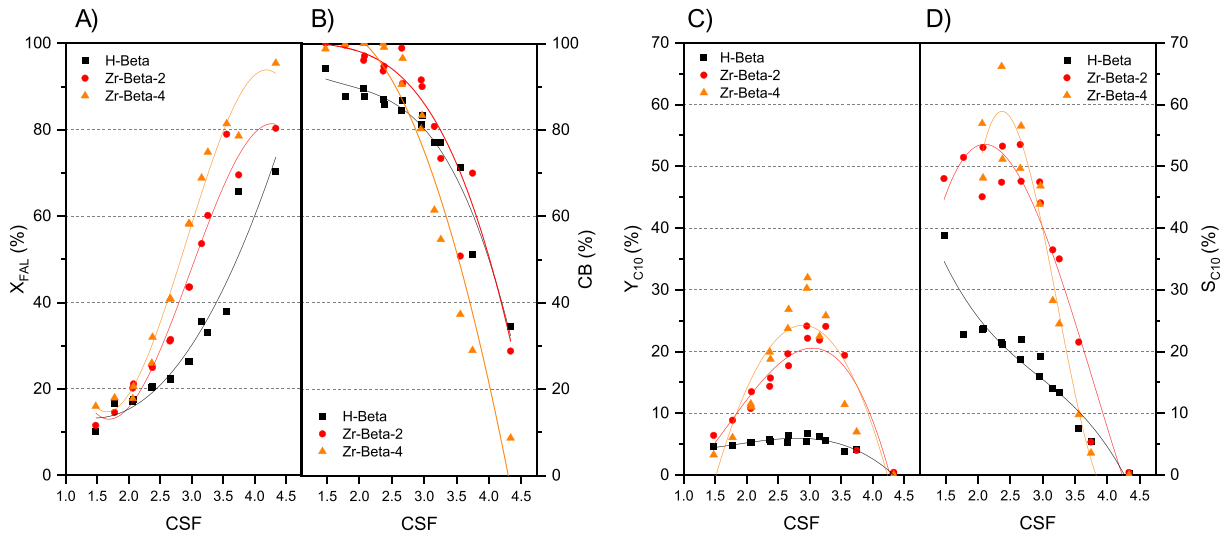

Fig. 4. Effect of the combined severity factor (CSF) in the X_{FAL} (A), CB (B), Y_{C10} (C), and S_{C10} (D) in the aldol condensation of FAL and LA over parent H-Beta zeolite, partially dealuminated Zr-modified Beta zeolite (Zr-Beta-2) and totally dealuminated Zr-modified Beta zeolite (Zr-Beta-4). Reaction conditions: LA/FAL (mol/mol) = 1, FAL/CAT (wt/wt) = 5.

with the highest Zr content) undesired side reactions are promoted, particularly under high-severity reaction conditions.

On the other hand, both selectivity and yield toward the desired C_{10} condensation adducts follow the same general trend: an initial increase with increasing CSF, the achievement of a maximum value, and a subsequent decrease beyond certain CSF thresholds (Fig. 4C–D). For these two response variables, a noticeable difference is observed when comparing the parent H-Beta zeolite with the Zr-modified Beta materials. In the case of H-Beta, the formation of the desired adducts is negligible regardless of the CSF value, whereas the Zr-modified Beta catalysts achieve maximum selectivity and yield at intermediate CSF values (CSF = 2.5 for selectivity and CSF = 3 for yield).

Accordingly, this study concludes that Zr-Beta-4 catalyst exhibits superior performance based on FAL conversion, carbon balance, and yield/selectivity to the target C_{10} adducts. This is attributed to the low B/L acid sites ratio and the almost complete absence of Al in this material (Table 1).

3.4.2. *Effect of the FAL dilution and catalyst loading*

Once the optimal catalyst and CSF values were identified, the influence of other reaction variables related to FAL dilution (LA/FAL molar ratio) and the FAL/CAT mass ratio, was investigated. To this end, a factorial experimental design combined with response surface methodology was applied [37]. Two temperature-time combinations were selected to achieve the required CSF values: 100 °C for 4 h (CSF = 2.5) and 120 °C for 4 h (CSF = 3). Consequently, two 3^2 factorial experimental designs were carried out using the best performing catalyst, Zr-Beta-4, with the aim of identifying reaction conditions that maximize FAL conversion while maintaining the highest selectivity towards the desired C_{10} adducts. The lower and upper level of the experimental factors were selected based on previous experiments: LA/FAL molar ratio (X_1) was analysed in the range from 1 to 9 while the studied FAL/CAT mass ratio (X_2) ranges from 2.5 to 7.5. The full experimental matrices for the aldol condensation of FAL and LA are reported in Tables S3 and S4, including the real factor values, their dimensionless coded levels (+1 for the highest and −1 for the lowest), and the corresponding experimental results. The experimental designs enable a comprehensive assessment of the effects of the factors on the response variables while simultaneously identifying factors interactions. In this work the FAL conversion (X_{FAL}), yield to C_{10} (Y_{C10}), and selectivity to C_{10} (S_{C10}) where chosen as response variables. Four replicates at the central point (0,0) were carried out to evaluate system reproducibility and estimate experimental error (runs 5-8 of Tables S3 and S4).

Assuming second-order polynomial behaviour, predictive equations (Eqs [7]. - [12], Table 2) were obtained by multiple regression analysis using Statgraphics software, relating each response to the independent variables X_1 and X_2, through linear and quadratic terms, as well as their binary interactions, expressed in coded form. The regression coefficients of the mathematical models (R^2) indicate a good agreement between the experimental data and the values predicted by the statistical models, supporting their validity. Among the three responses, selectivity showed the poorest fit, which can be attributed to the fact that it is derived from both conversion and yield, and consequently inherits the accumulated experimental error of these two variables.

In addition, analytical variability was evaluated using the center points. The averages values and corresponding standard deviations were: $X_{FAL} = 20.5 \pm 1.6\%$, $Y_{C10} = 13.8 \pm 2.0\%$ and $S_{C10} = 67.0 \pm 4.3\%$ for CSF = 2.5, and $X_{FAL} = 60.9 \pm 2.2\%$, $Y_{C10} = 39.4 \pm 2.8\%$ and $S_{C10} = 64.7 \pm 4.5\%$ for CSF = 3. Thus, all standard deviations were below 2.5% for conversion and yield, and below 4.5% for selectivity, which is indicative of a good reproducibility of the experimental system.

Fig. 5 depicts the surface response plots obtained for both experimental designs. As displayed, working under more moderate conditions allows higher selectivity to be achieved, at the expense of lower FAL

Table 2
Predictive model equations obtained by response surface methodology for the aldol condensation of FAL and LA over Zr-Beta-4.

Statistical models for a CSF of 2.5 (T = 100 °C; t = 4 h)	**R^2**	**Eq.**
$X_{FAL}(\%) = 20.2646 - 3.18333 * X_1 - 6.7 * X_2 + 1.01125 * X_1^2 + 4.0075 * X_1 * X_2 + 2.90125 * X_2^2$	0.975	[7]
$Y_{C10}(\%) = 13.9088 - 1.035 * X_1 - 5.46667 * X_2 - 0.47625 * X_1^2 + 0.835 * X_1 * X_2 + 1.62875 * X_2^2$	0.942	[8]
$S_{C10}(\%) = 67.9988 + 3.615 * X_1 - 6.10333 * X_2 - 3.40625 * X_1^2 - 6.68 * X_1 * X_2 - 2.52125 * X_2^2$	0.832	[9]
Statistical models for a CSF of 3 (T = 120 °C; t = 4 h)	**R^2**	**Eq.**
$X_{FAL}(\%) = 63.5429 + 0.165 * X_1 - 9.63333 * X_2 - 5.36875 * X_1^2 + 4.6625 * X_1 * X_2 + 1.12625 * X_2^2$	0.934	[10]
$Y_{C10}(\%) = 39.9725 + 6.5 * X_1 - 8.12333 * X_2 - 5.2275 * X_1^2 + 1.795 * X_1 * X_2 - 0.3175 * X_2^2$	0.916	[11]
$S_{C10}(\%) = 63.2213 + 11.255 * X_1 - 4.76 * X_2 - 3.34375 * X_1^2 + 0.615 * X_1 * X_2 - 2.89875 * X_2^2$	0.850	[12]

Note: X_1, coded value for LA/FAL molar ratio; X_2, coded value for FAL/Cat mass ratio; X_{FAL}, conversion of FAL; Y_{C10}, yield to C10; S_{C10}, selectivity to C_{10}.

conversion (Fig. 5A). In contrast, both FAL conversion and yield toward C_{10} products are superior when operating at a greater CSF (Fig. 5B).

By analysing the statistical models and the response surface plots, it can be deduced that the most influential factor affecting both X_{FAL} and Y_{C10} is the linear FAL/CAT ratio term (X_2), with a negative effect. This indicates that a decrease in this ratio leads to an increase in the response variables. Hence, a higher catalyst loading promotes FAL conversion and enhanced production of aldol condensation adducts. In contrast, the factors governing the selectivity toward the desired products depend on the CSF. For reactions carried out at 100 °C, the most influential factor is the interaction between the two factors ($X_1 \cdot X_2$), whereas under more severe conditions, the LA/FAL ratio (X_1) becomes the dominant factor influencing the selectivity to desired products.

For the CSF of 2.5, the reactant molar ratio appears to have a limited influence in the fitted models, as indicated by the nearly horizontal profile of the response surface plots. Additionally, the interaction between LA/FAL ratio and FAL/Cat ratio ($X_1 \cdot X_2$) has also been identified to be a significant factor, suggesting a different evolution of the FAL conversion and the yield to C_{10} with the catalyst loading at low and high LA/FAL ratio. On the other hand, for the CSF of 3, the quadratic term of LA/FAL molar ratio (X_1^2) is also significant, indicating that the increase in this factor does not lead to a linear rise in the response variables, which can be attributed to a significant curvature effect. Moreover, the linear LA/FAL ratio (X_1) appears as a significant factor affecting both the yield and selectivity toward the desired C_{10} adducts, exhibiting a positive effect. This fact indicates that under more severe operating conditions, it is important to work with a higher excess of LA in order to minimize the promotion of secondary reactions.

Overall, based on the results obtained from both experimental designs at different CSF values, it can be concluded that a reaction temperature of 120 °C is the most appropriate. Under these conditions, higher catalytic activity and higher yields are achieved, while in most cases maintaining selectivities comparable to those obtained at 100 °C. The optimal values of the response variables were X_{FAL} = 75.2%, and Y_{C10} = 48.8% at 120 °C, X_1 = 0.45 and X_2 = −1. Overall, optimization of the reaction conditions led to a clear improvement in all the response variables evaluated in this study. Notably, considering the solvent-free nature of the system, the optimization proved successful and resulted in robust performance of the cross-aldol condensation reaction.

3.5. Stability of the catalyst

The reusability of the Zr-Beta-4 catalyst was evaluated through recycling experiments. The following reaction conditions, close to those providing the best performance, were selected: LA/FAL molar ratio = 9, FAL/CAT mass ratio = 2.5, 120 °C and 4 h. After each reaction cycle, the catalyst was recovered by filtration, followed by washing with acetone and drying overnight. According to the results (Fig. 6), both catalytic activity and yield remained practically constant after three consecutive reaction cycles, demonstrating good stability under the reaction conditions investigated. The slight decrease observed in Y_{C10} after consecutive cycles is within the experimental variability of the system. However, a minor contribution from the accumulation of furfural-derived organic deposits on the catalyst surface cannot be excluded. As previously reported for related Zr-containing zeolitic catalysts [38], such deactivation would be expected to be reversible through calcination in air.

For comparison purposes, Table S5 summarizes the main catalytic systems reported in the literature for the aldol condensation of furfural and levulinic acid, including catalyst type, reaction conditions, and catalytic performance indicators. The comparison highlights that

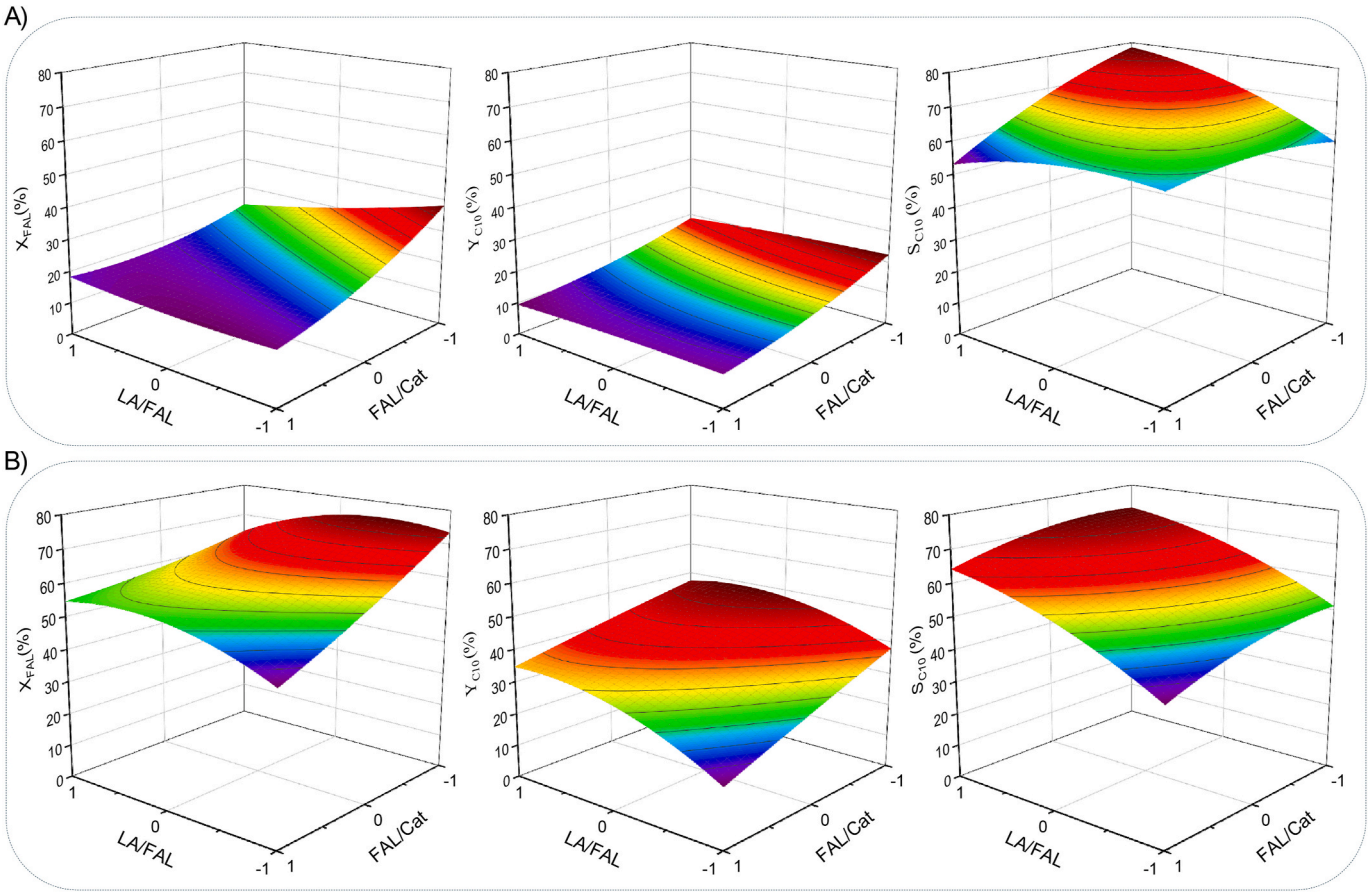

Fig. 5. Model-predicted response surfaces for FAL conversion, yield to the desired condensation adducts, and selectivity to the desired condensation adducts in the aldol condensation of FAL and LA over Zr-Beta-4. A) CSF = 2.5; B) CSF = 3.

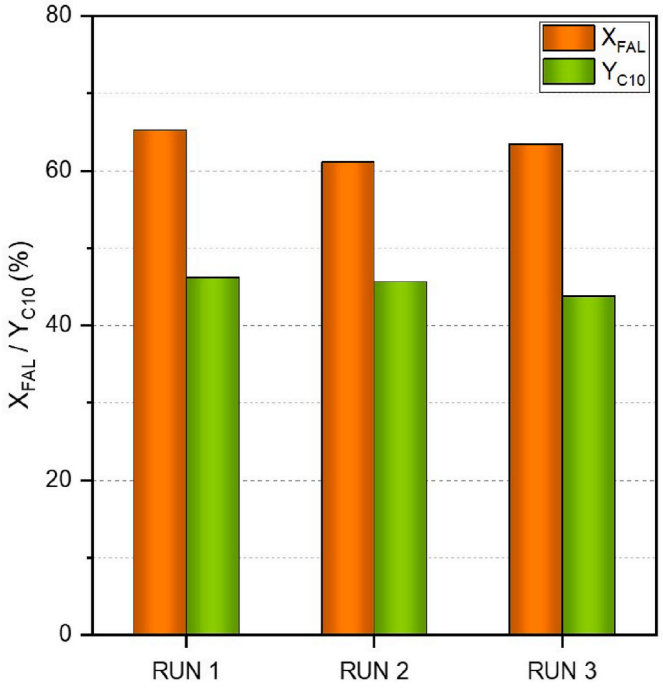

Fig. 6. Reusability of Zr-Beta-4 catalyst in three consecutive reaction cycles in the aldol condensation of FAL and LA. Reaction conditions: LA/FAL (mol/mol) = 9; FAL/CAT (wt/wt) = 2.5; T = 120 °C; t = 4 h.

competitive C10 yields can be achieved under solvent-free conditions while avoiding solvent handling and neutralization/reacidification steps required in many previously reported processes.

4. Conclusions

The catalytic performance of Beta zeolites in the solvent-free aldol condensation of FAL and LA is strongly governed by their acidic properties. Progressive dealumination and Zr incorporation markedly enhance catalytic performance, by decreasing the Brønsted/Lewis acid site ratio and promoting Lewis acidity, which enhances the formation of the desired C_{10} condensation products while suppressing undesired side reactions. Among the materials studied, the almost fully dealuminated Zr-Beta-4 catalyst exhibited the best overall performance achieving the highest furfural conversion, carbon balance, and C_{10} yield. Under optimized conditions (LA/FAL molar ratio = 6.8, FAL/Cat mass ratio = 2.5, 120 °C, 4 h), furfural conversion and C_{10} yield reached 75.2% and 48.8%, respectively. In addition, Zr-Beta-4 shows good stability upon reuse, maintaining activity and yield over consecutive cycles without the need for intermediate calcination, highlighting its robustness and potential for sustainable biomass upgrading.

CRediT authorship contribution statement

Natalia Uricochea: Writing – original draft, Methodology, Investigation, Data curation. **Jennifer Cueto:** Writing – review & editing, Methodology, Investigation. **María del Mar Alonso-Doncel:** Writing – review & editing, Methodology, Investigation. **Gabriel Morales:** Writing – review & editing, Validation, Supervision, Methodology, Investigation, Funding acquisition, Conceptualization. **Marta Paniagua:** Writing – original draft, Supervision, Methodology, Investigation, Data curation, Conceptualization. **Juan A. Melero:** Writing – review & editing, Validation, Supervision, Resources, Methodology, Investigation, Funding acquisition, Data curation, Conceptualization.

Acknowledgements

Financial support from the Spanish Ministry of Science and Innovation, through the projects SAFADCAT and BIOCATFLY, grant number PID2021- 122334OB-I00 and PID2024-157003OB-C21, are gratefully acknowledged.

Appendix A. Supplementary data

Supplementary data to this article can be found online at https://doi.org/10.1016/j.biombioe.2026.110093.

Data availability

Data will be made available on request.

References

[1] European Aviation Environmental Report 2019, Publications Office of the European Union, 2019.
[2] Hannah Förster, Christian Nissen, Anne Siemons, Nele Renders, Suzanne Dael, Melanie Sporer, Mihai Tomescu, Trends and Projections in Europe 2021, 2021, https://doi.org/10.2800/80374. Copenhagen, Denmark.
[3] Directive (EU) 2018/2001 of the European Parliament and of the Council, Off. J. Eur. Union (2018).
[4] IATA, Aviation Net-Zero CO2 Transition Pathways, 2024.
[5] IATA, Fact Sheet 2 Sustainable Aviation Fuel: Technical Certification, 2021.
[6] A. Bauen, N. Bitossi, L. German, A. Harris, K. Leow, Sustainable aviation fuels status, challenges and prospects of drop-in liquid fuels, hydrogen and electrification in aviation, Johnson Matthey Technol. Rev. 64 (2020) 263–278, https://doi.org/10.1595/205651320x15816756012040.
[7] A.H. Tanzil, K. Brandt, M. Wolcott, X. Zhang, M. Garcia-Perez, Strategic assessment of sustainable aviation fuel production technologies: yield improvement and cost reduction opportunities, Biomass Bioenergy 145 (2021), https://doi.org/10.1016/j.biombioe.2020.105942.
[8] P. Yan, H. Wang, Y. Liao, C. Wang, Zeolite catalysts for the valorization of biomass into platform compounds and biochemicals/biofuels: a review, Renew. Sustain. Energy Rev. 178 (2023) 113219, https://doi.org/10.1016/j.rser.2023.113219.
[9] X. Zhang, Y.Q. Li, C. Qian, L. An, W. Wang, X.F. Li, X.Z. Shao, Z. Li, Research progress of catalysts for aldol condensation of biomass based compounds, RSC Adv. 13 (2023) 9466–9478, https://doi.org/10.1039/D3RA00906H.
[10] E. de Jong, H. Stichnothe, G. Bell, M. Henning Jørgensen, I. de Bari, E. Jacco van Haveren, J. Lindorfer, Bio-based Chemicals A 2020 Update Bio-based Chemicals with Input From: (Pdf Version) Published by IEA Bioenergy, 2020.
[11] E. Cousin, K. Namhaed, Y. Pérès, P. Cognet, M. Delmas, H. Hermansyah, M. Gozan, P.A. Alaba, M.K. Aroua, Towards efficient and greener processes for furfural production from biomass: a review of the recent trends, Sci. Total Environ. 847 (2022) 157599, https://doi.org/10.1016/j.scitotenv.2022.157599.
[12] A.S. Amarasekara, T.B. Singh, E. Larkin, M.A. Hasan, H.J. Fan, NaOH catalyzed condensation reactions between levulinic acid and biomass derived furan-aldehydes in water, Ind. Crops Prod. 65 (2015) 546–549, https://doi.org/10.1016/j.indcrop.2014.10.005.
[13] C. Li, D. Ding, Q. Xia, X. Liu, Y. Wang, Conversion of raw lignocellulosic biomass into branched long-chain alkanes through three tandem steps, ChemSusChem 9 (2016) 1712–1718, https://doi.org/10.1002/cssc.201600386.
[14] M. Su, W. Li, Q. Ma, S. Li, T. Yang, X. Dou, Efficient synthesis of liquid fuel intermediates from furfural and levulinic acid via Aldol condensation over hierarchical MFI zeolite catalyst, Energy Fuel. 33 (2019) 12518–12526, https://doi.org/10.1021/acs.energyfuels.9b03307.
[15] G. Liang, A. Wang, X. Zhao, N. Lei, T. Zhang, Selective aldol condensation of biomass-derived levulinic acid and furfural in aqueous-phase over MgO and ZnO, Green Chem. 18 (2016) 3430–3438, https://doi.org/10.1039/c6gc00118a.
[16] J. Cueto, V. Korobka, L. Faba, E. Diáz, S. Ordóñez, Aldol condensation of biomass-derived levulinic acid and furfural over acid zeolites, ACS Sustain. Chem. Eng. 8 (2020) 4371–4383, https://doi.org/10.1021/acssuschemeng.9b06636.
[17] J. Cueto, L. Faba, E. Díaz, S. Ordóñez, From lignocellulosic biomass to chemical precursors: simultaneous valorization of furfural and levulinic acid over mesoporous acid catalysts, Ind. Crops Prod. 188 (2022) 115692, https://doi.org/10.1016/j.indcrop.2022.115692.
[18] J.A. Melero, G. Morales, J. Iglesias, M. Paniagua, C. López-Aguado, K. Wilson, A. Osatiashtiani, Efficient one-pot production of γ-valerolactone from xylose over zr-al-beta zeolite: rational optimization of catalyst synthesis and reaction conditions, Green Chem. 19 (2017) 5114–5121, https://doi.org/10.1039/C7GC01969F.
[19] V. Zholobenko, C. Freitas, M. Jendrlin, P. Bazin, A. Travert, F. Thibault-Starzyk, Probing the acid sites of zeolites with pyridine: quantitative AGIR measurements of the molar absorption coefficients, J. Catal. 385 (2020) 52–60, https://doi.org/10.1016/J.JCAT.2020.03.003.
[20] J.T. Scanlon, D.E. Willis, Calculation of flame ionization detector relative response factors using the effective carbon number concept, J. Chromatogr. Sci. 23 (1985) 333–340, https://doi.org/10.1093/CHROMSCI/23.8.333.

[21] J.W. Harris, M.J. Cordon, J.R. Di Iorio, J.C. Vega-Vila, F.H. Ribeiro, R. Gounder, Titration and quantification of open and closed lewis acid sites in Sn-Beta zeolites that catalyze glucose isomerization, J. Catal. 335 (2016) 141–154, https://doi.org/10.1016/J.JCAT.2015.12.024.
[22] K. Gołabek, S. Kurucová, J.F. Miñambres, K. Veselá, T. Zakeri, J. Přech, Zr-Site lewis acidity determines terpenoid reduction selectivity, ACS Catal. 16 (2026) 3307–3318, https://doi.org/10.1021/ACSCATAL.5C07220.
[23] F. Lónyi, J. Valyon, A TPD and IR study of the surface species formed from ammonia on zeolite H-ZSM-5, H-mordenite and H-beta, thermochim, Acta 373 (2001) 53–57, https://doi.org/10.1016/S0040-6031(01)00458-0.
[24] L. Qi, Y. Zhang, M.A. Conrad, C.K. Russell, J. Miller, A.T. Bell, Ethanol conversion to butadiene over isolated zinc and yttrium sites grafted onto dealuminated beta zeolite, J. Am. Chem. Soc. 142 (2020) 14674–14687, https://doi.org/10.1021/jacs.0c06906.
[25] E. Peeters, S. Calderon-Ardila, I. Hermans, M. Dusselier, B.F. Sels, Toward industrially relevant Sn-BETA zeolites: synthesis, activity, stability, and regeneration, ACS Catal. 12 (2022) 9559–9569, https://doi.org/10.1021/acscatal.2c02527.
[26] A.A. Khechfe, T.B.M. Matha, Y. Román-Leshkov, Solvent polarity and framework hydrophobicity of Hf-BEA zeolites influence aldol addition rates in organic media, ACS Catal. 13 (2023) 6474–6485, https://doi.org/10.1021/acscatal.3c00787.
[27] B. Hernández, J. Iglesias, G. Morales, M. Paniagua, C. López-Aguado, J.L. García Fierro, P. Wolf, I. Hermans, J.A. Melero, One-pot Cascade transformation of xylose into γ-valerolactone (GVL) over bifunctional Brønsted–Lewis Zr–Al-beta zeolite, Green Chem. 18 (2016) 5777–5781, https://doi.org/10.1039/C6GC01888B.
[28] S.K.R. Patil, C.R.F. Lund, Formation and growth of humins via aldol addition and condensation during acid-catalyzed conversion of 5-Hydroxymethylfurfural, Energy Fuel. 25 (2011) 4745–4755, https://doi.org/10.1021/EF2010157.
[29] E. de Jong, M. Mascal, S. Constant, T. Claessen, P. Tosi, A. Mija, The origin, composition, and applications of industrial humins – a review, Green Chem. 27 (2025) 3136–3166, https://doi.org/10.1039/D4GC06244B.
[30] K.D. Kim, J. Kim, W.Y. Teoh, J.-C. Kim, J. Huang, R. Ryoo, Cascade reaction engineering on zirconia-supported mesoporous MFI zeolites with tunable Lewis–Brønsted acid sites: a case of the one-pot conversion of furfural to γ-valerolactone, RSC Adv. 10 (2020) 35318–35328, https://doi.org/10.1039/d0ra06915a.
[31] J.D. Lewis, S. Van De Vyver, Y. Román-Leshkov, Acid-base pairs in lewis acidic zeolites promote direct aldol reactions by soft enolization, Angew. Chem. Int. Ed. 54 (2015) 9835–9838, https://doi.org/10.1002/ANIE.201502939.
[32] W. Fang, S. Liu, L. Schill, M. Kubus, T. Bligaard, A. Riisager, On the role of Zr to facilitate the synthesis of diesel and jet fuel range intermediates from biomass-derived carbonyl compounds over aluminum phosphate, Appl. Catal., B 320 (2023) 121936, https://doi.org/10.1016/J.APCATB.2022.121936.
[33] A.S. Amarasekara, T.B. Singh, E. Larkin, M.A. Hasan, H.-J. Fan, NaOH catalyzed condensation reactions between levulinic acid and biomass derived furan-aldehydes in water, Ind. Crops Prod. 65 (2015) 546–549, https://doi.org/10.1016/J.INDCROP.2014.10.005.
[34] J. Cueto, L. Faba, E. Díaz, S. Ordóñez, From lignocellulosic biomass to chemical precursors: simultaneous valorization of furfural and levulinic acid over mesoporous acid catalysts, Ind. Crops Prod. 188 (2022) 115692, https://doi.org/10.1016/J.INDCROP.2022.115692.
[35] L. Chen, Y. Liu, X. Zhang, J. Liu, Q. Zhang, L. Ma, Catalytic production of long-chain hydrocarbons suitable for aviation turbine fuel from biomass-derived levulinic acid and furfural, Fuel 334 (2023) 126665, https://doi.org/10.1016/J.FUEL.2022.126665.
[36] M. Su, W. Li, Q. Ma, S. Li, T. Yang, X. Dou, Efficient synthesis of liquid fuel intermediates from furfural and levulinic acid via aldol condensation over hierarchical MFI zeolite catalyst, Energy Fuel. 33 (2019) 12518–12526, https://doi.org/10.1021/acs.energyfuels.9b03307.
[37] G.E.P. Box, J.S. Hunter, W.G. Hunter, Statistics for Experimenters: Design, Innovation, and Discovery, second ed., Wiley.
[38] N. Uricochea, V. Uzquiano, M. Paniagua, G. Morales, J.A. Melero, Zr-modified USY zeolite as an efficient catalyst for the production of bio-jet fuel precursors from levulinic acid and furfural in the absence of solvent, Catal. Today 450 (2025) 115211, https://doi.org/10.1016/J.CATTOD.2025.115211.